IEEE Access
Multidisciplinary | Rapid Review | Open Access Journal

Received March 16, 2018, accepted April 21, 2018, date of publication April 26, 2018, date of current version May 24, 2018.

Digital Object Identifier 10.1109/ACCESS.2018.2830415

RMapCS: Radio Map Construction From Crowdsourced Samples for Indoor Localization

YANZHEN YE AND BANG WANG
School of Electronic Information and Communications, Huazhong University of Science and Technology, Wuhan 430074, China
Corresponding author: Bang Wang (wangbang@hust.edu.cn)

This work was supported by the National Natural Science Foundation of China under Grant 61771209.

ABSTRACT Fingerprint crowdsourcing has recently been promoted as a promising solution for fingerprinting-based indoor localization systems to relieve the burden of site survey. When constructing an indoor localization map from crowd-sourced samples, the following challenges should be addressed: inaccurate sample annotation, unequal sample dimensionality, measurement device diversity, and nonuniform spatial distribution. In this paper, we propose the radio map construction from crowd-sourced sample (RMapCS) scheme to handle these challenges. The RMapCS consists of four main modules: outlier detection, source selection, fingerprint interpolation, and device calibration. For each device in each grid, we first propose an improved clustering algorithm to remove outliers and use a threshold-based approach to select only those important signal sources. For a grid without enough samples, we propose a fingerprint interpolation algorithm to construct its device-specific fingerprints. Then, we propose a device calibration algorithm to fuse samples from different devices to obtain grid fingerprints. We also propose a two-step online positioning algorithm consisting of both set comparison and similarity computation. We conduct field measurements and experiments to examine the localization performance. Results show that the proposed RMapCS can achieve significant improvements over the peer schemes and the average localization error can achieve around 1.5 m by using only the received signal strength-based fingerprints.

INDEX TERMS Indoor localization map construction, sample crowdsoucing, outlier detection and removal, source selection, fingerprint interpolation, device calibration.

I. INTRODUCTION

Location information plays a very important role in numerous industrial and commercial applications, such as mobile robots [1], construction industry [2], pedestrian tracking [3], [4], and etc. Due to the poor performance of Global Positioning System (GPS) in indoor environments, many research efforts have been devoted to design *indoor positioning systems* (IPSs) based on *received signal strength* (RSS) from the *access points* (APs) in *wireless local area networks* (WLANs) [5]–[7].

In the last decade, the *fingerprinting* technique has been extensively researched for most RSS-based IPSs [8]–[10]. The basic idea is based on the assumption that each indoor spatial location possesses an unique signal feature, dubbed as *fingerprint*. The location of a test fingerprint can be estimated to a known location with the minimal signal space distance. To support the signal distance comparison, an indoor *radio map* should be first constructed, which consists of the training fingerprints each for one *reference point* (RP) with known location. To construct a radio map, site survey can be used to collect RSS samples each measured at an RP by some professional surveyor. However, site survey is too time-consuming, labor-intensive and cost-prohibitive to be implemented for large environments.

To help reducing or even eliminating the burdensome site survey, the crowdsourcing approach has been recently promoted to construct a radio map from *crowdsourced samples*, i.e., the samples casually collected at non-specified locations from crowd [6], [11]–[14]. Compared with the site survey, crowdsourcing distributes the tedious work of sample measurement to common users rather than only professional surveyors, by which labor cost and time can be reduced. However, some new challenges arise when constructing radio maps from crowdsourced samples:

- *Inaccurate sample annotation*: Crowdsourced samples are generally not collected at specified locations, yet each still needs to be annotated with some location information for radio map construction. Such annotations are

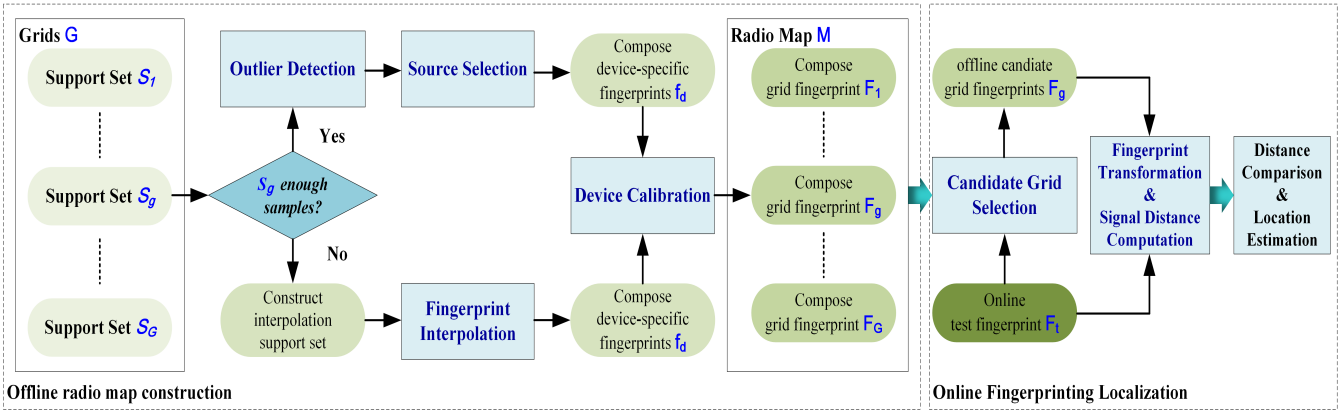

FIGURE 1. The proposed system diagram. The offline radio map M consists of the grid fingerprints in each subarea. For each grid, we first decide whether it is a sufficiency or deficiency one according to the size of its support set $\mathcal{S}$. For a sufficiency grid, we perform the outlier detection and source selection and then compose its device-specific fingerprints f. For a deficiency grid, we apply the fingerprint interpolation technique to obtain its device-specific fingerprints f. We then perform the device calibration to compose the grid fingerprint F for all grids. In the online positioning phase, we first select a subset of candidate grids according to the number of mutually hearable APs by the test fingerprint F_t and a grid fingerprint F_g. We then apply the proposed fingerprint transformation for both F_t and F_g and compute their signal distance. Finally, the center of a grid with the smallest signal distance is output as the estimated location.

often inaccurate, which could lead to inaccurate radio maps.

- *Unequal sample dimensionality*: For casual collections, it may happen that different samples may contain different hearable sources due to the variations of radio transmission and/or the differences of body direction, even if they are actually collected at the same location.
- *Measurement device diversity*: As common users normally possess various brands and types of smartphones, different radio chips and antenna designs may lead to different measurement values of the samples collected the same source even at the same location and time.
- *Nonuniform spatial distribution*: As the crowdsourcing process is often not with some standard nor mandate procedure, it may happen that the crowdsourced samples are not uniformly distributed in the whole indoor environment, some areas are with many samples; While some others contain few or even no crowdsourced samples.

In this paper, we propose a radio map construction scheme based on crowdsourced samples to solve the above four problems. We first divide an indoor environment into several distinct subareas, each of which is further divided into non-overlapping grid cells with almost equal sizes. The objective is to compose a *grid fingerprint* for each grid and then construct the radio map for each subarea. For each grid, we propose to maintain a *support set* containing its crowdsourced samples, which can be represented as a *data cube*. Fig. 1 presents the proposed system diagram, and Fig. 2 illustrates the data processing flow. The proposed offline system consists of the following modules: (i) *outlier detection* (OD); (ii) *source selection* (SS); (iii) *fingerprint interpolation* (FI) and (iv) *device calibration* (DC). For each module, we propose a corresponding data processing algorithm, by which we process the raw data cube and compose each grid fingerprint. In the online phase, we propose a fingerprint transformation algorithm and a two-step positioning algorithm to obtain the estimated location for an online test fingerprint. We have conducted extensive experiments based on practical field measurements for five different smartphone types. Experiment results validate the proposed system in terms of improved localization accuracies in most practical scenarios.

We briefly summarize our contributions as follow:

- Propose a new system diagram to construct a radio map from crowdsourced samples;
- Design four algorithms to address the four challenges of sample crowdsourcing;
- Propose a fingerprint transformation and two-step online positioning algorithm;
- Conduct field experiments to examine the performance of our proposed scheme.

The remainder of the paper is organized as follows. Section II reviews the related work. Our proposed solution is presented in Section III and IV, and evaluated via field experiments in Section V. Section VI concludes the paper.

II. RELATED WORK

Some previous schemes have been proposed to construct radio map based on the crowdsourced samples obtained from pedestrian trajectories [15]–[18]. Kim *et al.* [15] propose to use trajectory samples to enhance a radio map based on the lightweight site survey, i.e., using only a few of RP fingerprints. Zhou *et al.* [16] apply a semi-supervised manifold alignment approach to construct a radio from crowdsourced movement trajectories together with some specially calibrated fingerprints. Besides using crowdsourced trajectory samples, some have also proposed to exploit some landmarks, like the cross points of corridors, detected in trajectories to calibrate a radio map [17], [18]. However, these schemes have not considered the four challenges discussed in the previous section.

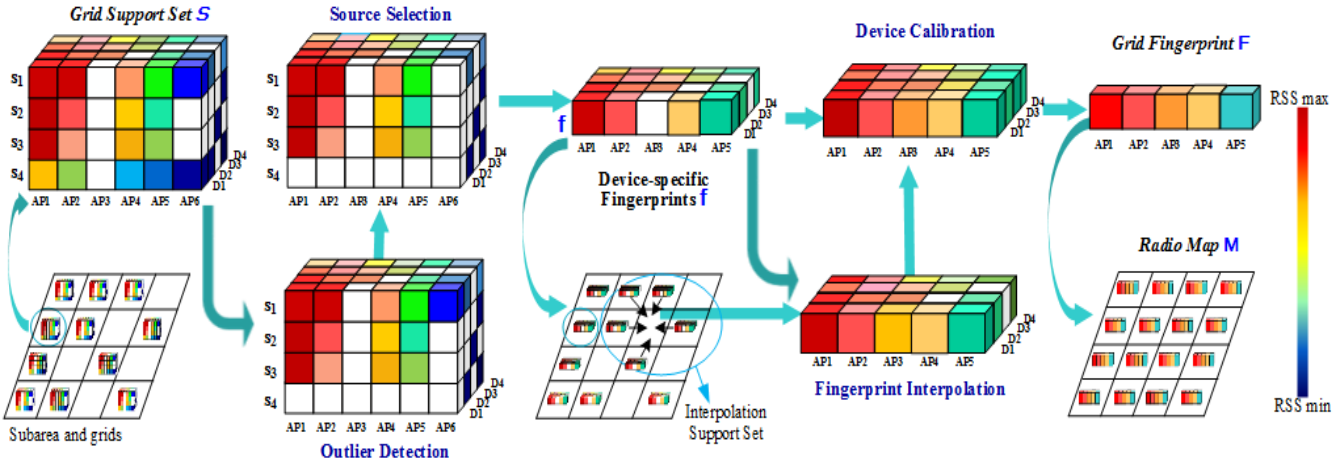

FIGURE 2. Illustration of the data processing procedure of the proposed system. Each grid maintains a support set $\mathcal{S}$ as illustrated by a colored cube. Each slice of the cube represents the samples from a particular device, and each row in a slice represents a sample, viz., a RSS vector. Each colored unit in a row represents the RSS value from an AP, yet a white unit indicates that the corresponding AP is not hearable in this sample. The data cube is processed as follows: After the per-device outlier detection, the sample s_4 is removed for device D_1; After the per-device source selection, the AP AP_6 is removed for device D_1; The device-specific fingerprints f are composed for each device; For a deficiency grid, the device-specific fingerprints are obtained via the fingerprint interpolation; After the device calibration, the grid fingerprint F is composed for each grid and the radio map M is constructed for a subarea.

Some previous work have studied one or two of the four challenges, such as addressing the inaccurate sample annotation [8], nonuniform spatial distribution [19] and unequal sample dimensionality [20]–[22]. In [8], a bottom-up hierarchical clustering approach has been used to distinguish the correctly labeled samples from all the samples in a trajectory. However, the hierarchical clustering suffers from the random initial sample selection, which may render a cluster mainly containing mislabeled samples. In [19], the *log-distance path loss* (LDPL) model is adopted to reconstruct a fingerprint for such a grid without samples. However, the estimation based on the LDPL model is often not accurate in complex indoor environments due to the *non-line-of-sight* (NLOS) problem. Laitinen and Lohan [21] have examined several AP selection strategies, including the KL-based, dissimilarities-based, maxRSS-based and entropy-based selection. They report that the maxRSS-based one seems to offer the best localization performance among others. However, only utilizing the maxRSS AP could decrease discrimination capability of crowdsourced samples.

Several approaches have been proposed to solve the device diversity problem recently, which can be generally classified into two categories: *inter-device calibration* [19], [23]–[26] and *intra-device transformation* [6], [27]–[35]. In inter-device calibration, the basic idea is based on the assumption that some linear relation exists in between the reception gains of any two transceivers. For example, in [19], the gain offset has been proposed to calibrate the signal space distance between any pair of fingerprints between different devices. However, this approach generally demands huge efforts for offline sample collection and computation. In intra-device transformation, the basic idea is to transform the original RSS value vector into a device-independent fingerprint. For example, in [28]–[30], the difference or ratio in between two elements in a RSS vector has been used as the transformed fingerprint, which, however, significantly increases the RSS vector dimensionality. To solve the dimension expansion problem, some researchers have proposed to only use the RSS offset to a particular AP [31] or to use the RSS offset to the mean RSS value [32], and some researchers have proposed to compare absolute RSS values at nearby positions to build a gradient-based fingerprint map [35]. However, these schemes have not considered the fusion of crowdsourced samples from different devices.

In this paper, we design a novel diagram for radio map construction from crowdsourced samples and solve the four challenges through our algorithms of outlier detection, source selection, fingerprint interpolation and device calibration.

III. MapCS: RADIO MAP CONSTRUCTION FROM CROWDSOURCED SAMPLES

A. THE MapCS OVERVIEW

We first divide an indoor environment into several distinct subareas, such as rooms, corridors and etc, according to their functional layouts by inherent obstructions and partitions like concrete walls. For each subarea, we create a lattice structure consisting of non-overlapping grid cells. For site survey, samples are collected on each grid center via surveyors to compose the *grid fingerprint*, and all grid fingerprints consist of an indoor radio map. For crowdsourcing, we define a *support set* for one grid which contains the crowdsourced samples each with its annotated location within the grid. The objective is to compose each grid a fingerprint for constructing the indoor radio map M for each subarea. Table 1 presents the main symbols and their meanings in the paper hereafter.

The proposed MapCS scheme first constructs a grid fingerprint from its support set. Let $\mathcal{S}$ and $\mathbf{F}$ denote the support

TABLE 1. Key symbols and their notations.

Symbol	Definition
M	The indoor radio map
$\mathcal{S}$	The support set of a grid
$\mathcal{S}_d = \{\mathbf{s}_1, ..., \mathbf{s}_N\}$	The set of samples measured by the device d, where $\mathbf{s}_i$ is the RSS vector
$\mathcal{S}_d^n$, $\mathcal{S}_d^o$	The normal and the outlier set of the dth device
$\mathbb{R}^{(0)}$, $\mathbb{R}^{(1)}$, $\mathbb{R}^{(2)}$, $\mathbb{R}^{(3)}$	The original RSS matrix for one device, the RSS matrix after completing the outlier detection for one device, the RSS matrix after the source selection for one device and the RSS matrix after filling the missing RSS values for one device
N, $N^{(1)}$, $N^{(2)}$	The total number of available samples for one device, the number of samples after completing the outlier detection for one device and the number of samples after the source selection for one device
M, $M^{(1)}$, $M^{(2)}$, $M^{(3)}$	The total number of all hearable APs for one device, the number of APs after completing the outlier detection for one device, the number of APs after the source selection for one device and the number of APs after filling the missing RSS values for all devices
N_d	The number of available devices
$\mathcal{F} = \{\mathbf{f}^1, ..., \mathbf{f}^d, ..., \mathbf{f}^{N_d}\}$	The set of device-specific fingerprints
$\mathbf{f}_g^d = (r_1, ..., r_{M_2})$	The device-specific fingerprint from the dth device in the grid g
$\mathbf{F}$, $\mathbf{F}_g$, $\mathbf{F}_t$	The grid fingerprint of a grid, the grid fingerprint in grid g and the online testing fingerprint
$\mathbf{F}_t^{int}$, $\mathbf{F}_g^{int}$	The test fingerprint and the grid fingerprint consisting of RSS values only from those mutually hearable APs in the intersection set $\mathcal{A}^{int}$, respectively
$\widetilde{\mathbf{F}}_t$, $\widetilde{\mathbf{F}}_g$	The transformed fingerprints for $\mathbf{F}_t$ and $\mathbf{F}_g$, respectively
$\mathcal{A}^{uni}$, $\mathcal{A}^{int}$	The union set and the intersection set of hearable APs, respectively
$\mathcal{A}_i$, $\mathcal{A}^t$, $\mathcal{A}^g$	The set of hearable APs in $\mathbf{s}_i$, $\mathbf{F}_t$ and $\mathbf{F}_g$, respectively
r_{nm}	The RSS value received from the mth AP by the nth sample for one device.
r_m	The averaged RSS for the mth AP from all samples for one device
r_{gm}^d	The RSS value for the mth AP in device-specific fingerprint $\mathbf{f}_g^d$ in the grid g by the device d
$\hat{r}_m^d$	The interpolated RSS for the mth AP for the device d
r_m^d	The averaged RSS for the mth AP from the dth device
$\bar{r}_m$	The averaged RSS value from all devices that can hear the mth AP
$\tilde{r}_m^d$	The calibrated value for the mth AP for the dth device
r_{gm}, r_{tm}	The RSS value of the mth AP in $\mathbf{F}_g$ and $\mathbf{F}_t$, respectively
$\bar{r}_t$, $\bar{r}_g$	The mean value of $\mathbf{F}_t^{int}$ and $\mathbf{F}_g^{int}$, respectively
$d_{nn'}$, d_c	The signal distance between two samples n and n' and the cutoff distance, respectively
ρ_n, ρ_{th}	The local density of the nth sample and the density threshold, respectively
$\mathcal{B}_n$	The set of neighbors for the nth sample
N_m	The number of non-empty elements in the mth column in $\mathbb{R}^{(1)}$
P_m,P_{th}	The acceptance ratio of the mth AP and the acceptance ratio threshold, respectively
$\mathcal{G}$, $\mathcal{G}_{iss}$	The set of all grids in one subarea and the interpolation support set
D_g, $\mathcal{D}$	The set of supported devices in one grid $g \in \mathcal{G}_{iss}$ and in $\mathcal{G}_{iss}$, respectively
K^d	The number of grid-distinct device-d fingerprints in the interpolation support set
γ	The interpolation support threshold
(x_g, y_g)	The coordinates of the gth grid center
ω_{cd}	The the polynomial coefficient
Δ^d	The calibration factor for the dth device
$\mathcal{D}_m$, $\overline{\mathcal{D}_m}$	the set of devices each of whose the corresponding r_m^d is missing and r_m^d exists, respectively
K_{tg}	The number of mutual hearable APs by $\mathbf{F}_t$ and $\mathbf{F}_g$
$D(\widetilde{\mathbf{F}}_t, \widetilde{\mathbf{F}}_g)$	The mean Euclidean distance between $\widetilde{\mathbf{F}}_t$ and $\widetilde{\mathbf{F}}_g$

set of a grid and its fingerprint, respectively. We note that $\mathcal{S}$ can be represented by a *data cube*. Each slice in a cube contains the samples collected by a particular smartphone brand and type (or called a *device* hereafter); While each row vector in a slice indicates a sample with each element the RSS value from a particular AP. The grid fingerprint $\mathbf{F}$ is a vector with each element the RSS from a particular AP. The first step is to compose $\mathbf{F}$ from $\mathcal{S}$ for each grid, if $\mathcal{S}$ contains enough samples. For a grid without enough crowdsourced samples, we create its fingerprint via the interpolation from its neighboring grids' fingerprints.

The proposed MapCS consists of the following four modules: (1) outlier detection, (2) source selection, (3) fingerprint interpolation and (4) device calibration. We first divide all grids into two categories: *sufficiency* and *deficiency*. A sufficiency grid contains enough samples for at least one device type; Yet a deficiency grid does not contain enough samples even for one device type. For a crowdsourced grid, we first detect and remove outliers from $\mathcal{S}$, if they exist. Among all hearable APs, we then select a subset of them to compose device-specific fingerprints, denoted by $\mathbf{f}$. Next, we calibrate diverse devices by fusing multiple device-specific fingerprints into a single device-independent grid fingerprint. Last, we interpolate a fingerprint for each deficiency grid. Furthermore, we improve the online positioning algorithm by including a source selection and fingerprint transformation algorithm before fingerprint matching.

Fig. 1 illustrates the system architecture and proposed modules for both offline radio map construction and online fingerprinting localization; While Fig. 2 illustrates the data

processing flow of the proposed scheme. Some discussions are also provided in the two figures.

B. OUTLIER DETECTION

This module is, for each sufficiency grid, to detect and remove those erroneously annotated samples. In this paper, a sample is called *normal*, if it is measured at the location within its annotated grid; Otherwise, it is an *outlier*. When composing a grid fingerprint, the hearable AP set is composed by those APs appearing once or more times in its samples. Furthermore, the averaging technique or distribution estimation is normally performed over the samples for each hearable AP. Therefore, including outliers has at least two negative impacts: changing the set of hearable APs of a grid and deviating the averaged RSS values from their respective ground truth values.

Since we do not have the ground truth labels for crowdsourced samples, an unsupervised machine learning algorithm like clustering is an appropriate choice for outlier detection. Among many clustering algorithms, we choose the density-based one recently proposed by Rodriguez and Laio [36], which clusters samples according to their similarity-based local density. For our problem, we argue that the similarity in between normal samples would be higher than that in between normal samples and outliers, and also higher than that in between outliers. Notice that the outlier detection is device-specific, that is, it is done for each slice in the data cube.

Let $\mathcal{S}_d = \{\mathbf{s}_1, \ldots, \mathbf{s}_N\}$ denote the set of samples measured by a particular device d, where each sample $\mathbf{s}_i$ is a RSS vector and N the total available samples. Let $\mathcal{A}_i$ denote the set of hearable APs in $\mathbf{s}_i$. Let $M = |\bigcup \mathcal{A}_i|$ denote the total number of all hearable APs in $\mathcal{S}_d$. Note that M and N may be different across different devices and different girds. We construct a $N \times M$ RSS matrix $\mathbb{R}^{(0)}$ for each device, in which an element r_{nm} is the RSS value received from the mth AP by the nth sample. The signal distance between two samples is computed by $d_{nn'} = \sqrt{\sum_{m \in \mathcal{A}_{nn'}^{int}} (r_{nm} - r_{n'm})^2}$, where $\mathcal{A}_{nn'}^{int} = \mathcal{A}_n \bigcap \mathcal{A}_{n'}$ is the set of hearable APs by both samples. The smaller the signal distance $d_{nn'}$, the more similar of the two samples.

We also define two thresholds, namely, the *cutoff distance* d_c and the *density threshold* ρ_{th} according to [36]. Since the number of samples and their pairwise distances of $\mathcal{S}_d$ may be much different in different grid for different devices, we set $\rho_{th} = \eta \times N$ and set d_c as the β percentile distance of all the $N \times N$ pairwise distances sorted in an ascending order. A sample $\mathbf{s}_n$ is called a *neighbor* of another sample $\mathbf{s}_{n'}$, if $d_{nn'} < d_c$. Let $\mathcal{B}_n = \{n' | d_{nn'} < d_c\}$ denote the set of neighbors for the nth sample. The *local density* of the sample is defined as the number of neighbors, $\rho_n = |\mathcal{B}_n|$. Based on the clustering algorithm [36], a sample $\mathbf{s}_n$ is detected as an outlier, if $\rho_n < \rho_{th}$; Otherwise, it is a normal sample.

In this paper, we extend the above onetime outlier detection into an iterative one. The pseudo-codes of the proposed algorithm are presented in **Algorithm 1**. At first, we classify each sample into either the normal set $\mathcal{S}_d^n$ or the outlier set $\mathcal{S}_d^o$ based on its local density. While there exists an outlier in $\mathcal{S}_d^o$, we pop an outlier $\mathbf{s}'$ and update the neighbors of each normal sample $\mathbf{s}_i \in \mathcal{S}_d^n$. Notice that after this update, the local density of $\mathbf{s}_i$ may become smaller than the density threshold ρ_{th}. In this case, this sample $\mathbf{s}_i$ is also detected as an outlier and is pushed into $\mathcal{S}_d^o$. The iteration terminates until $\mathcal{S}_d^o = \emptyset$.

Algorithm 1 Iterative Outlier Detection Based on Clustering

Require: The set of samples $\mathcal{S}_d$
Ensure: The normal set $\mathcal{S}_d^n$

```
Compute d_nn' between all sample pairs in S_d
Sort the N × N distances d_nn' into d
Compute d_c as the β percentile distance of d
Compute B_n and ρ_n for each s_n ∈ S_d
Set S_d^n = S_d, S_d^o = ∅
Cluster each s_n ∈ S_d into S_d^n (S_d^o) based on ρ_n ≥ ρ_th (ρ_n < ρ_th)
while S_d^o ≠ ∅ do
    Pop a sample s' from S_d^o
    for each sample s_i ∈ S_d^n do
        if s' ∈ B_i  then B_i = B_i \ {s'}
        if |B_i| ≤ ρ_th then S_d^n = S_d^n \ {s_i}, S_d^o = S_d^o ⋃ {s_i}
    end for
end while
Return S_d^n
```

For each grid, since we do not have the priori knowledge about how many outliers could exist, we usually set a moderate density threshold ρ_{th} according to the number of available samples, like $0.3N$. If a sample $\mathbf{s}_i$ is detected as an outlier, its neighbor $\mathbf{s}_j$ might also be outlier if their distance are small. On the other hand, it is also possible that $\mathbf{s}_j$ is still be detected as normal due to its local density $\rho_j > \rho_{th}$ in the first iteration, which, however, has included an outlier $\mathbf{s}_i$ into the density computation. This issue could be addressed if we recompute the local density in each iteration after removing a detected outlier. We note that in our problem the false positive is considered as more serious than the false negative. That is, we would rather remove a normal being detected as an outlier, than include an outlier being detected as normal.

After completing the outlier detection, we use $\mathcal{S}_d^n$ to denote the set of normal samples and construct a new $N^{(1)} \times M^{(1)}$ RSS matrix $\mathbb{R}^{(1)}$ for each device in a grid.

C. SOURCE SELECTION

This module is, for each sufficiency grid, to select a subset of APs to compose device-specific fingerprints. The number of hearable APs in $\mathcal{S}_d^n$ could be very large in many typical indoor environments. For example, in a campus lecture building, a sample can hear more than 100 different APs according to our field measurements. On the one hand, not all APs are hearable by every sample even by the same device due to the variations of radio propagation and/or obstructions of body

direction. On the other hand, it may still exist unremoved outliers in $\mathcal{S}_d^n$, which may introduce undesirable APs, weakening the fingerprint discrimination capability. We next propose a source selection algorithm to select only a subset of hearable APs to compose a device-specific fingerprint.

The source selection is based on the AP acceptance ratio as follows. Let N_m denote the number of non-empty elements in the mth column in $\mathbb{R}^{(1)}$, which indicates the mth AP heard by N_m samples. The acceptance ratio of the mth AP is defined as $P_m = N_m/N^{(1)}$. We also define an acceptance ratio threshold P_{th}. If $P_m < P_{th}$, then the mth AP is not included into the device-specific fingerprint composition. That is, the mth column of $\mathbb{R}^{(1)}$ is removed.

After the source selection, we construct a new $N^{(2)} \times M^{(2)}$ RSS matrix $\mathbb{R}^{(2)}$, where an element r_{nm} is the crowdsourced RSS from the mth AP in the nth sample. In this paper, we adopt the commonly used RSS averaging approach to compose device-specific fingerprints $\mathbf{f}$ for each grid. That is, we compute the averaged RSS for the mth AP by $r_m = \frac{1}{|r_{\cdot m}|}\sum_{n=1}^{N^{(2)}} r_{nm}$, where $r_{\cdot m}$ is the mth column vector of $\mathbb{R}^{(2)}$. The device-specific fingerprint is then construct as $\mathbf{f} = (r_1, \ldots, r_{M^{(2)}})$.

D. FINGERPRINT INTERPOLATION

This module is to, for each deficiency grid, interpolate its device-specific fingerprints from its surrounding sufficiency grids within the same subarea. Due to the casual collection nature, some grids contain only a few or even none crowdsourced samples. For example, the center pathway of a corridor is with higher likelihood to collect many samples compared with the corridor edges. We next present a fingerprint interpolation algorithm based on the surface fitting technique.

The pseudo-codes are presented in **Algorithm 2**. Let $\mathcal{G}$ denote the set of all grids in one subarea. For one deficiency grid in the subarea, we construct an *interpolation support set* $\mathcal{G}_{iss}$ from its surrounding grids as follows: Starting from an empty set of $\mathcal{G}_{iss}$, we first include one of its direct neighboring grids into $\mathcal{G}_{iss}$. The function **includeOneSurroundingGrid**$(\mathcal{G}_{iss}, g)$ is to include a surrounding grid $g \in \mathcal{G}\backslash\mathcal{G}_{iss}$ into $\mathcal{G}_{iss}$, while the grid g is a directly neighboring grid of either the deficiency grid or any grid in $\mathcal{G}_{iss}$. Let D_g and $\mathcal{D} = \bigcup_{g\in\mathcal{G}_{iss}} D_g$ denote the set of supported devices in one grid $g \in \mathcal{G}_{iss}$ and that in $\mathcal{G}_{iss}$, respectively. Note that each device $d \in D_g$ has a device-specific fingerprint $\mathbf{f}_g^d$ in the grid g. We use the function **countSupportFingerprint**$(\mathcal{D}, d)$ to return the number of grid-distinct device-d fingerprints in the interpolation support set, denoted by K^d. We define an *interpolation support threshold* γ as a small integer. If $\mathcal{G}\backslash\mathcal{G}_{iss} \neq \emptyset$ or none of device $d \in \mathcal{D}$ contains more than γ grid-distinct device-d fingerprints, the construction process continues by including another surrounding grid. Otherwise, the $\mathcal{G}_{iss}$ construction terminates.

After the construction process, for each device $d \in \mathcal{D}$, if $K^d > \gamma$, we perform the fingerprint interpolation as

Algorithm 2 Fingerprint Interpolation for a Deficiency Grid

```
Set finished=FALSE, G_iss = ∅
while not finished and G\G_iss ≠ ∅ do
    Update G_iss=includeOneSurroundingGrid(G_iss, g)
    Update the set of devices D
    for each d ∈ D do
        Compute K^d =countSupportFingerprint(D, d)
        if K^d > γ then finished=TRUE, break
    end for
end while
for each d ∈ D with K^d > γ do
    Compute A^d = ⋂_{g∈G_iss} A_g^d
    for each m ∈ A^d do
        Construct φ_m(·) according to Eq. (1) and (2)
        Compute r̂_m^d = φ_m(·)
    end for
    Compose an interpolated fingerprint f_g^d = (r̂_m^d)_{m∈A^d}
end for
```

follows: Let $\mathcal{A}_g^d$ denote the set of hearable APs by the device d in grid $g \in \mathcal{G}_{iss}$. Let $\mathcal{A}^d = \bigcap_{g\in\mathcal{G}_{iss}} \mathcal{A}_g^d$ be the set of APs to perform the fingerprint interpolation for the deficiency grid. For each AP $m \in \mathcal{A}^d$, we first construct a RSS surface $\phi_m(x_g, y_g)$ to minimize the following sum of squared error based on the least square principle:

$$\text{minimize } \theta \equiv \sum_{g\in\mathcal{G}_{iss}, m\in\mathcal{A}^d} (\phi_m(x_g, y_g) - r_{gm}^d)^2, \qquad (1)$$

where (x_g, y_g) are the coordinates of the gth grid center and r_{gm}^d is the RSS value in the grid g device-specific fingerprint $\mathbf{f}_g^d$ by the device d from the mth AP. We adopt a binary polynomial function to construct the surface fitting function ϕ_m as follows:

$$\phi_m(x, y) = \sum_{c=1}^{p}\sum_{d=1}^{q} \omega_{cd} x^{c-1} y^{d-1}, \qquad (2)$$

where ω_{cd}s are the polynomial coefficients and let $(p, q) = (2, 2)$ avoid over-fitting and to reduce computation complexity. Notice that the input of ϕ_m is a location and output is a RSS value. Therefore, the interpolated RSS $\hat{r}_m^d$ from the AP m by the device d is interpolated as the output of ϕ_m for the deficiency grid. Accordingly, we can interpolate all the RSS values for other APs in $\mathcal{A}^d$ and compose the interpolated device-specific fingerprint(s) for the deficiency grid.

Some discussions are as follows: The interpolation is done in a per-device and per-AP manner for each deficiency grid. In the construction of $\mathcal{G}_{iss}$, we do not try to include as many as possible of surrounding grids for fingerprint interpolation. Instead, we just find enough grid-distinct fingerprints for the interpolation of at least one device. We argue that using too many surrounding grids, especially farther away from the deficiency grid, could introduce larger RSS deviations seen

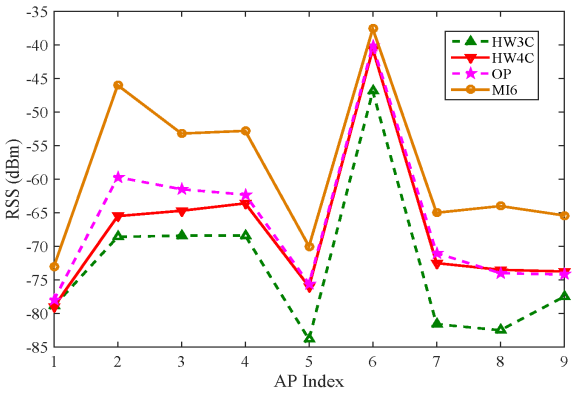

FIGURE 3. Field measurements of RSS values from nine APs by different devices at the same measurement location.

by the deficiency grid, since radio propagation variations generally increase with the increase of the transmission distance. Notice that it is possible that after the construction, no device in $\mathcal{G}_{iss}$ satisfies $K^d > \gamma$, that is, no device contains enough fingerprints for interpolation. In this case, we simply do not create interpolated fingerprints for the deficiency grid.

E. DEVICE CALIBRATION

This module is, for each grid, to calibrate different device-specific fingerprints and fuse them into a single grid fingerprint. As crowdsourced samples could be contributed by many different smartphone brands and types in practice, it could cost lots of computation and storage resource to establish multiple grid fingerprints each for one particular device. Event worse, it could happen that an online testing fingerprint is issued by a smartphone that had not been seen in the offline database. We next propose a new inter-device calibration algorithm based on the receiver pattern analysis.

At the same measurement location, the RSS r_m from the mth AP might be different across different devices due to that they have different receiver implementations of antennas and circuits, viz., different receiver gains. For example, for two devices $r_m^d - r_m^{d'} = \delta$ with δ the difference of their receiver gains. On the other hand, as the receiver gain takes effect on each hearable APs, so a *receiver pattern* can be observed. That is, if $r_m^d - r_m^{d'} = \delta$, it might be most likely that $r_{m'}^d - r_{m'}^{d'} \simeq \delta$ for another AP also. Fig. 3 plots the field RSS measurements at the same location by using different devices. It can observe that the RSS values for two devices exhibit a similar difference across different APs, though with some small variation possibly due to measurement noises.

In this paper, we propose to exploit the receiver pattern from two aspects: calibrating missing values in the offline phase and transforming positioning fingerprints in the online phase. For one grid, let $\mathcal{F} = \{\mathbf{f}^1, \ldots, \mathbf{f}^d, \ldots, \mathbf{f}^{N_d}\}$ denote the set of device-specific fingerprints. Again, let $\mathcal{A}^d$ denote the set of hearable APs by the dth device, which may be different across different devices. Let $\mathcal{A}^{uni} = \bigcup_{d=1}^{N_d} \mathcal{A}^d$ and $\mathcal{A}^{int} = \bigcap_{d=1}^{N_d} \mathcal{A}^d$ be the *union set* and *intersection set* of hearable APs, respectively, from all available N_d device types. Let $\overline{\mathcal{A}^d} = \mathcal{A}^{uni} - \mathcal{A}^d$ denote the *complement set* of unhearable APs by the dth device. Let $M^{(3)} = |\mathcal{A}^{uni}|$ denote the number of total hearable APs from different devices. We note that each device-specific fingerprint $\mathbf{f}^d = (r_1^d, \ldots, r_m^d, \ldots, r_{M^{(3)}}^d)$ is supposed to be with $M^{(3)}$ RSS values, which, however, is often not the case due to the device diversity problem. Some r_m^d in $\mathbf{f}^d$ might be missing, if the mth AP is not hearable by the dth device.

In the offline phase, we propose to calibrate the missing values as follows. Let $\bar{r}_m = \frac{1}{N_d} \sum_{d=1}^{N_d} r_m^d$, $m \in \mathcal{A}^{int}$, denote the averaged RSS value from all devices that can hear the mth AP. For each device, we define a *calibration factor* Δ^d by

$$\Delta^d = \frac{1}{|\mathcal{A}^{int}|} \sum_{m \in \mathcal{A}^{int}} (r_m^d - \bar{r}_m), \quad d = 1, \ldots, N_d. \tag{3}$$

The inter-device fingerprint calibration is done for each AP $m \in \mathcal{A}_{uni} - \mathcal{A}_{int}$. Let $\mathcal{D}_m$ denote the set of devices each of whose the corresponding r_m^d is missing, and let $\overline{\mathcal{D}_m}$ denote its complement set, i.e., each device $d \in \overline{\mathcal{D}_m}$ has the corresponding r_m^d value. The fingerprint calibration for such an AP m is to compute the calibrated value of $\tilde{r}_m^d$ for all $d \in \mathcal{D}_m$ from the following linear equations:

$$\tilde{r}_m^d - \frac{1}{N_d} \left(\sum_{d \in \overline{\mathcal{D}_m}} r_m^d + \sum_{d \in \mathcal{D}_m} \tilde{r}_m^d \right) = \Delta^d, \quad d \in \mathcal{D}_m. \tag{4}$$

Note that if $|\mathcal{D}_m| = L$, then we have in total L such linear equations and each equation contains L unknowns. Furthermore, $|\mathcal{D}_m| < N_d$ and $|\mathcal{D}_m| \geq 1$. Therefore, we can always compute a unique $\tilde{r}_m^d$ for each device $d \in \mathcal{D}_m$. That is, a missing value r_m^d is filled by the inter-device calibrated value of $\tilde{r}_m^d$. We propose device calibration to calibrate the missing value(s) when composing a device-specific fingerprint. The following is the proof of the existence and uniqueness of a solution $\tilde{r}_m^d$:

1) THE EXISTENCE OF THE SOLUTION

Based on the radio propagation model, the RSS from the mth AP received by a smartphone type d can be written as:

$$r_m^d = P_m^{act} + 10 \log G_r^d + Z_m^d, \tag{5}$$

where $P_m^{act} = P_t + 10 \log \frac{G_t \lambda^2}{(4\pi)^2} - 10\alpha \log(d_m/d_0)$ is the actual signal strength without considering the effect of reception gain G_r and random noise, and Z_m^d is the value of random noise. P_t is the signal transmission power in dBm. The average RSS of the intersection set $\bar{r}_m$ can be further written as follows:

$$\bar{r}_m = \frac{1}{N_d} \sum_{d=1}^{N_d} r_m^d = P_m^{act} + \frac{10}{N_d} \log \bar{G}_r + \bar{Z}_m, \tag{6}$$

where $\bar{G}_r = \prod_{d=1}^{N_d} G_r^d$ and $\bar{Z}_m = \frac{1}{N_d} \sum_{d=1}^{N_d} Z_m^d$. Theoretically, the RSS not received by the dth device from the mth AP is:

$$\tilde{r}_m^d = P_m^{act} + 10 \log G_r^d + Z_m^d. \tag{7}$$

Based on Eq. (5) and (6), Eq. (3) in the paper can be written as:

$$\begin{aligned}\Delta^d &= \frac{1}{|\mathcal{A}^{int}|}\sum_{m\in\mathcal{A}^{int}}(r_m^d-\bar{r}_m)\\ &= \frac{1}{|\mathcal{A}^{int}|}\sum_{m\in\mathcal{A}_{int}}(10\log G_r^d-\frac{10}{N_d}\log\bar{G}_r+Z_m^d-\bar{Z}_m)\\ &= 10\log G_r^d-\frac{10}{N_d}\log\bar{G}_r+\frac{1}{|\mathcal{A}_{int}|}\sum_{m\in\mathcal{A}_{int}}(Z_m^d-\bar{Z}_m).\end{aligned}$$

Suppose Eq. (7) is the solution of linear equations (4) in the paper, the left of Eq. (4) is equal to $(10\log G_r^d-\frac{10}{N_d}\log\bar{G}_r+Z_m^d-\bar{Z}_m)$. Because the random noise is uncontrolled, if we do not consider the effect of random noise, the left of Eq. (4) is equal to the right Δ^d. Therefore, Eq. (7) is the solution of linear equations (4) and can better complement the RSS values for each device that does not hear the mth AP.

2) THE UNIQUENESS OF THE SOLUTION

We learn that the first L ($L < N_d$ and $L \geq 1$) devices do not hear the mth AP, so we have in total L linear equations from Eq. (4) and each equation contains L unknowns $(\tilde{r}_m^1, \tilde{r}_m^2, \cdots \tilde{r}_m^L)$. It can be written as:

$$(1-\frac{1}{N_d})\tilde{r}_m^l-\frac{1}{N_d}\sum_{l'=1,l'\neq l}^{L}\tilde{r}_m^{l'}=Q+\Delta^l,\quad l=1,\ldots,L. \tag{8}$$

where $Q = \frac{1}{N_d}\sum_{d\in\mathcal{D}_m} r_m^d$. Convert Eq. (8) into the form of matrix:

$$AX = Y, \tag{9}$$

where

$$\begin{aligned}A &= \begin{bmatrix}1-\frac{1}{N_d} & -\frac{1}{N_d} & \cdots & -\frac{1}{N_d}\\ -\frac{1}{N_d} & 1-\frac{1}{N_d} & \cdots & -\frac{1}{N_d}\\ \vdots & \vdots & \vdots & \vdots\\ -\frac{1}{N_d} & -\frac{1}{N_d} & \cdots & 1-\frac{1}{N_d}\end{bmatrix},\\ X &= \begin{bmatrix}\tilde{r}_m^1 & \tilde{r}_m^2 & \cdots & \tilde{r}_m^L\end{bmatrix}^T,\\ Y &= \begin{bmatrix}Q+\Delta^1 & Q+\Delta^2 & \cdots & Q+\Delta^L\end{bmatrix}^T,\end{aligned}$$

Since A is a full rank matrix,Eq. (9) has the unique solution. Combined the proof of the existence of solution, Eq. (7) is the unique solution of linear equations (4) and can better complement the RSS values for each device that does not hear the mth AP.

After filling the missing RSS values, we obtain $N_d \times M^{(3)}$ RSS matrix $\mathbb{R}^{(3)}$ with each element r_m^d either the original or calibrated RSS value of the dth from the mth AP. Note that $M^{(3)}$ and N_d may be different across different grids. By column-wise averaging of $\mathbb{R}^{(3)}$, we obtain the grid fingerprint $\mathbf{F}_g = (r_{g1}, \ldots, r_{gm}, \ldots, r_{gM^{(3)}})$, where $r_{gm} = \frac{1}{N_d}\sum_{d=1}^{N_d} r_m^d$, $r_m^d \in \mathbb{R}^{(3)}$. In the next section, we will further propose a fingerprint transformation algorithm for device calibration in the online phase.

IV. ONLINE POSITIONING ALGORITHM

We propose an improved *nearest neighbor* (NN) online positioning algorithm, which consists of two parts: candidate grid selection based on the number of mutual sources and target grid determination based on the comparison of distances between transformed fingerprints.

Let $\mathbf{F}_t = (r_{t1}, \ldots, r_{tm})$ and $\mathbf{F}_g = (r_{g1}, \ldots, r_{gm})$ denote the online testing fingerprint and the offline fingerprint of the gth grid, respectively. Note that both r_{tm} and r_{gm} take non-zero values. Let $\mathcal{A}^t$ and $\mathcal{A}^g$ denote the set of hearable APs by $\mathbf{F}_t$ and $\mathbf{F}_g$, respectively. Let $\mathcal{A}^{int} = \mathcal{A}^t \bigcap \mathcal{A}^g$ denote the AP intersection set of the two fingerprints. We first select candidate grids for distance computation as follows: Among all available grids, we select a candidate grid according to the number of mutual hearable APs, $K_{tg} \equiv |\mathcal{A}^{int}|$. In particular, we sort all available grids according K_{tg} in a decreasing order, and select the top ρ percentile grids as the candidate grids.

We first perform an online fingerprint transformation as follows: We continue using $\mathbf{F}_g$ to denote a candidate grid fingerprint. Let $\mathbf{F}_t^{int} = (r_{tm})_{m\in\mathcal{A}^{int}}$ and $\mathbf{F}_g^{int} = (r_{gm})_{m\in\mathcal{A}^{int}}$, respectively, denote the test and grid fingerprint consisting of RSS values only from those mutually hearable APs in the intersection set $\mathcal{A}^{int}$. The mean value of $\mathbf{F}_t^{int}$ and $\mathbf{F}_g^{int}$ are computed by

$$\bar{r}_t = \frac{1}{|\mathcal{A}^{int}|}\sum_{m\in\mathcal{A}^{int}} r_{tm} \quad \text{and } \bar{r}_g = \frac{1}{|\mathcal{A}^{int}|}\sum_{m\in\mathcal{A}^{int}} r_{gm}. \tag{10}$$

The transformed fingerprints for distance computation are computed by

$$\widetilde{\mathbf{F}}_t = \mathbf{F}_t^{int} - \bar{r}_t = (r_{tm}-\bar{r}_t)_{m\in\mathcal{A}^{int}}, \tag{11}$$

and

$$\widetilde{\mathbf{F}}_g = \mathbf{F}_g^{int} - \bar{r}_g = (r_{gm}-\bar{r}_g)_{m\in\mathcal{A}^{int}}. \tag{12}$$

We compute the signal distance as the mean Euclidean distance between the two fingerprints:

$$D(\widetilde{\mathbf{F}}_t, \widetilde{\mathbf{F}}_g) = \frac{1}{|\mathcal{A}^{int}|}\sqrt{\sum_{m\in\mathcal{A}^{int}}((r_{tm}-\bar{r}_t)-(r_{gm}-\bar{r}_g))^2}. \tag{13}$$

The target grid is determined by the one with the smallest signal distance and its grid center is selected as the estimated location for the test fingerprint.

Some discussions are as follows: Candidate grid selection, on the one hand, can reduce the online computation time, as only a subset of grids are needed to perform fingerprint transformation and comparison that are considered as requiring more computation effort than a simple operation of set intersection. On the other hand, we argue that selecting candidate grids with more mutually hearable APs could improve the confidence of distance comparison in between different grids. According to Eq. (13), the fingerprint distance is averaged over the number of mutually hearable APs. For example, if two grids g_1 and g_2 are with the same D to the test fingerprint, however, $|\mathcal{A}_{g_1}^{int}| = 1$ and $|\mathcal{A}_{g_2}^{int}| = 10$. We would put more trust to grid g_2, as sharing more

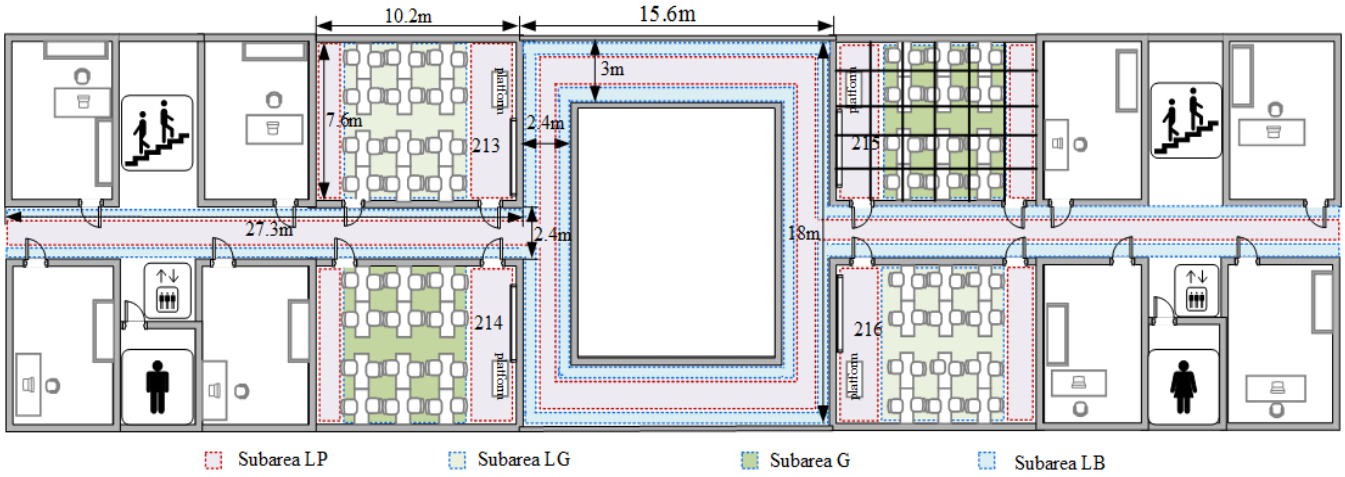

FIGURE 4. The layout of experiment environment. The total area is 592 m^2 and there are five subareas including four classrooms and one corridor. Each grid cell is with 0.6 × 0.6 m^2 area which is used to perform the site survey. In addition, we create deficiency grids according to the practical situations. There are five situations as follow: (E1) (46.9%): The middle of corridor and sides of four rooms illustrated as subarea LP; (E2a) (34.4%) The corridor and sides of room 213 and 216 illustrated as subarea LP+LG; (E2b) (34.4%) The corridor and sides of room 214 and 215 illustrated as subarea LP+G; (E3) (25%) The corridor and sides of four rooms illustrated as subarea LP+LB; (E4) (21.9%) The middle of corridor and full four rooms illustrated as subarea LP+LG+G.

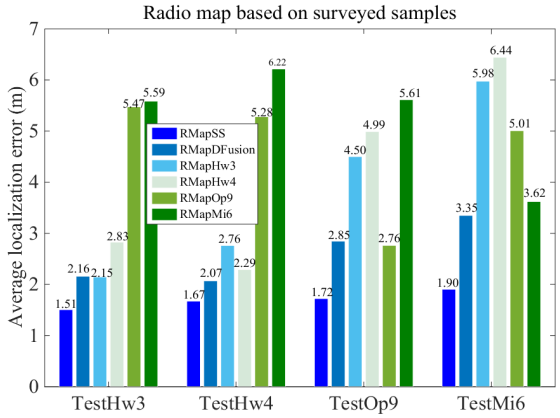

FIGURE 5. Comparison of ALE based on surveyed samples.

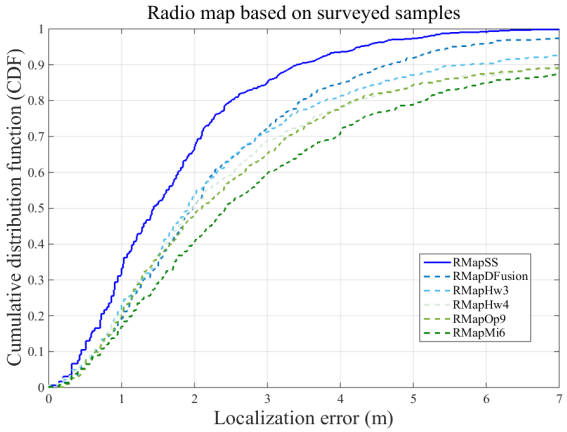

FIGURE 6. Comparison of CDF based on surveyed samples.

mutually hearable APs normally implies that the radio environment of grid g_2 is more like that of the test fingerprint, hence the higher likelihood of the true location for the test fingerprint.

We adopt both offline calibration and online transformation to solve the device diversity. Our arguments are as follows: For one grid, $\mathbf{F}_t = (r_{t1}, \ldots, r_{tm})$ and $\mathbf{F}_g = (r_{g1}, \ldots, r_{gm})$ are the online test fingerprint and the grid fingerprint at the gth grid, respectively, where

$$r_{tm} = P_{tm}^{act} + 10 \log G_r + Z_{tm}, \tag{14}$$

and the average RSS from the mth AP by different devices can be computed by:

$$r_{gm} = \frac{1}{N_d} \sum_{d=1}^{N_d} r_{gm}^d = P_{gm}^{act} + \frac{10}{N_d} \log \bar{\bar{G}}_r + \bar{\bar{Z}}_{gm}. \tag{15}$$

Due to offline calibration making each AP heard from multiple identical devices, the average receiver gain on the RSS of different devices as shown in Eq. (16) is the same for other APs in the same grid.

$$\frac{10}{N_d} \log \bar{\bar{G}}_r = \frac{10}{N_d} \log(\prod_{d=1}^{N_d} G_r^d). \tag{16}$$

The random noise of different device is:

$$\bar{\bar{Z}}_{gm} = \frac{1}{N_d} \sum_{d=1}^{N_d} Z_m^d. \tag{17}$$

During the online transformation, the mean value of $\mathbf{F}_t^{int}$ and $\mathbf{F}_g^{int}$ are computed by

$$\bar{r}_t = \frac{1}{|\mathcal{A}^{int}|} \sum_{m \in \mathcal{A}^{int}} P_{tm}^{act} + 10 \log G_r + \frac{1}{|\mathcal{A}^{int}|} \sum_{m \in \mathcal{A}^{int}} Z_{tm} \tag{18}$$

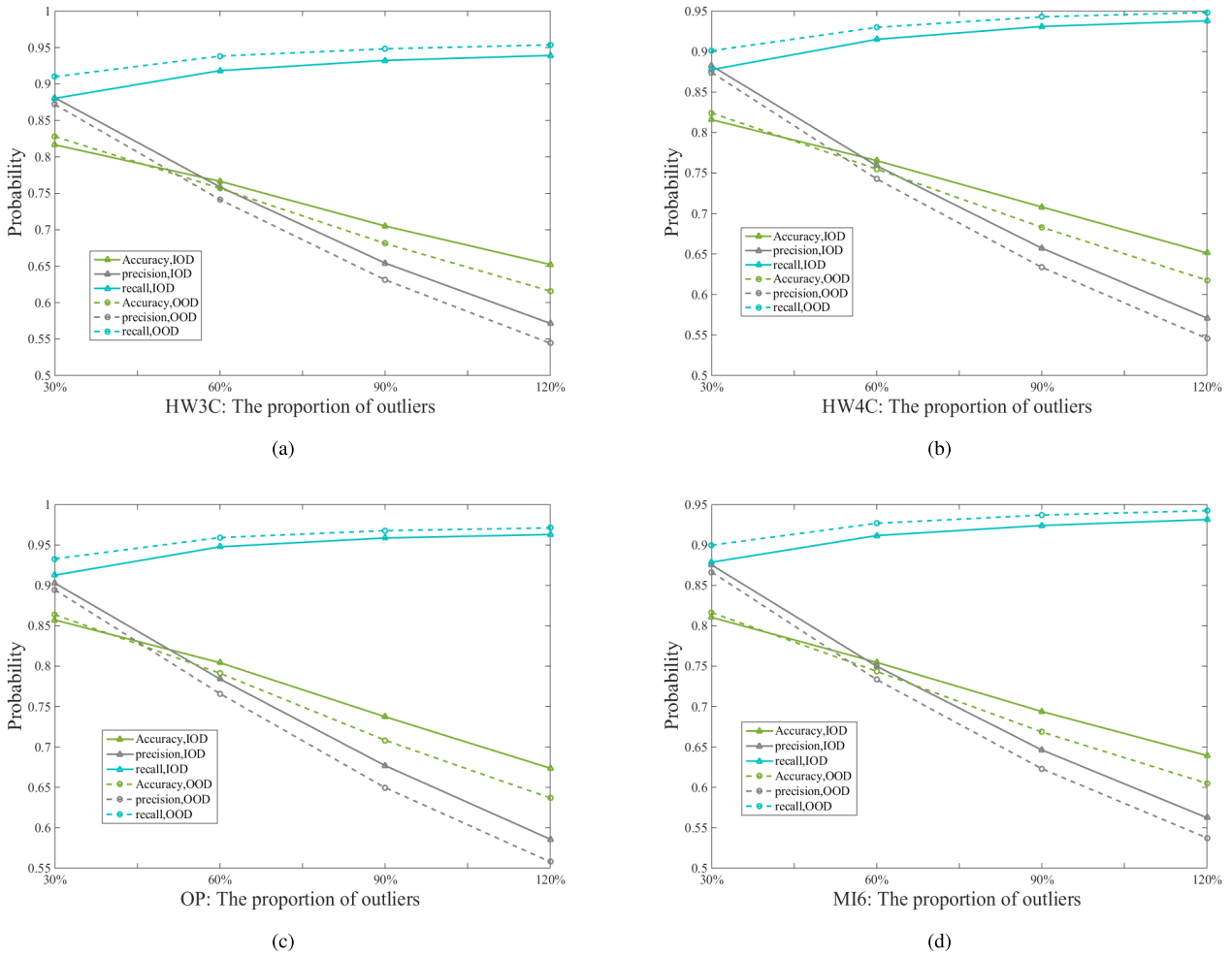

FIGURE 7. Comparison of the performance of outlier detection for different devices based on crowdsourced samples. (a) Outlier detection performance of device HW3C. (b) Outlier detection performance of device HW4C. (c) Outlier detection performance of device Op9. (d) Outlier detection performance of device Mi6

and

$$\bar{r}_g = \frac{1}{|\mathcal{A}^{int}|}\sum_{m\in\mathcal{A}^{int}} P_{gm}^{act} + \frac{10}{N_d}\log\bar{\bar{G}}_r + \frac{1}{|\mathcal{A}^{int}|}\sum_{m\in\mathcal{A}^{int}} \bar{\bar{Z}}_{gm}. \tag{19}$$

If not considering the effect of random noise, the transformed fingerprints $\widetilde{\mathbf{F}}_t$ and $\widetilde{\mathbf{F}}_g$ can be written as:

$$\widetilde{\mathbf{F}}_t = \mathbf{F}_t^{int} - \bar{r}_t = (P_{tm}^{act} - \frac{1}{|\mathcal{A}^{int}|}\sum_{m\in\mathcal{A}^{int}} P_{tm}^{act})_{m\in\mathcal{A}^{int}} \tag{20}$$

and

$$\widetilde{\mathbf{F}}_g = \mathbf{F}_g^{int} - \bar{r}_g = (P_{gm}^{act} - \frac{1}{|\mathcal{A}^{int}|}\sum_{m\in\mathcal{A}^{int}} P_{gm}^{act})_{m\in\mathcal{A}^{int}}. \tag{21}$$

The transformed fingerprints $\widetilde{\mathbf{F}}_t$ and $\widetilde{\mathbf{F}}_g$ are uncorrelated with receiver gains of different devices. Thus, the offline calibration and online transformation can solve the device diversity.

V. EXPERIMENT RESULTS

A. EXPERIMENT SETUP

We conducted field measurements in a typical office environment, as illustrated by Fig. 4. We used a lattice structure to obtain 1480 grids each about 0.6×0.6 m^2. Five different Android smartphones were used to obtain RSS measurements from existing WLAN APs, including Huawei Hol T00 (Hw3), Huawei CHM-TL00 (Hw4), Xiaomi MI6 (Mi6), Oppo R9sk (Op9) and Meizu MX5 (Mx5). We used the first four devices to obtain 10 samples in each grid and obtain in total 59, 200 training samples. For each device, we obtain 650 testing fingerprints that are evenly distributed within the experiment environment, and hence we obtain in total 3,250 testing fingerprints. The data collection continued for one week.

For each grid, we can construct two types of sample support sets: The surveyed one contains all the training samples measured within the grid; While the crowdsourced one contains both normal samples and outliers: The normal samples are the training samples in those grids whose centers are not more than 1m away from the given grid center. The

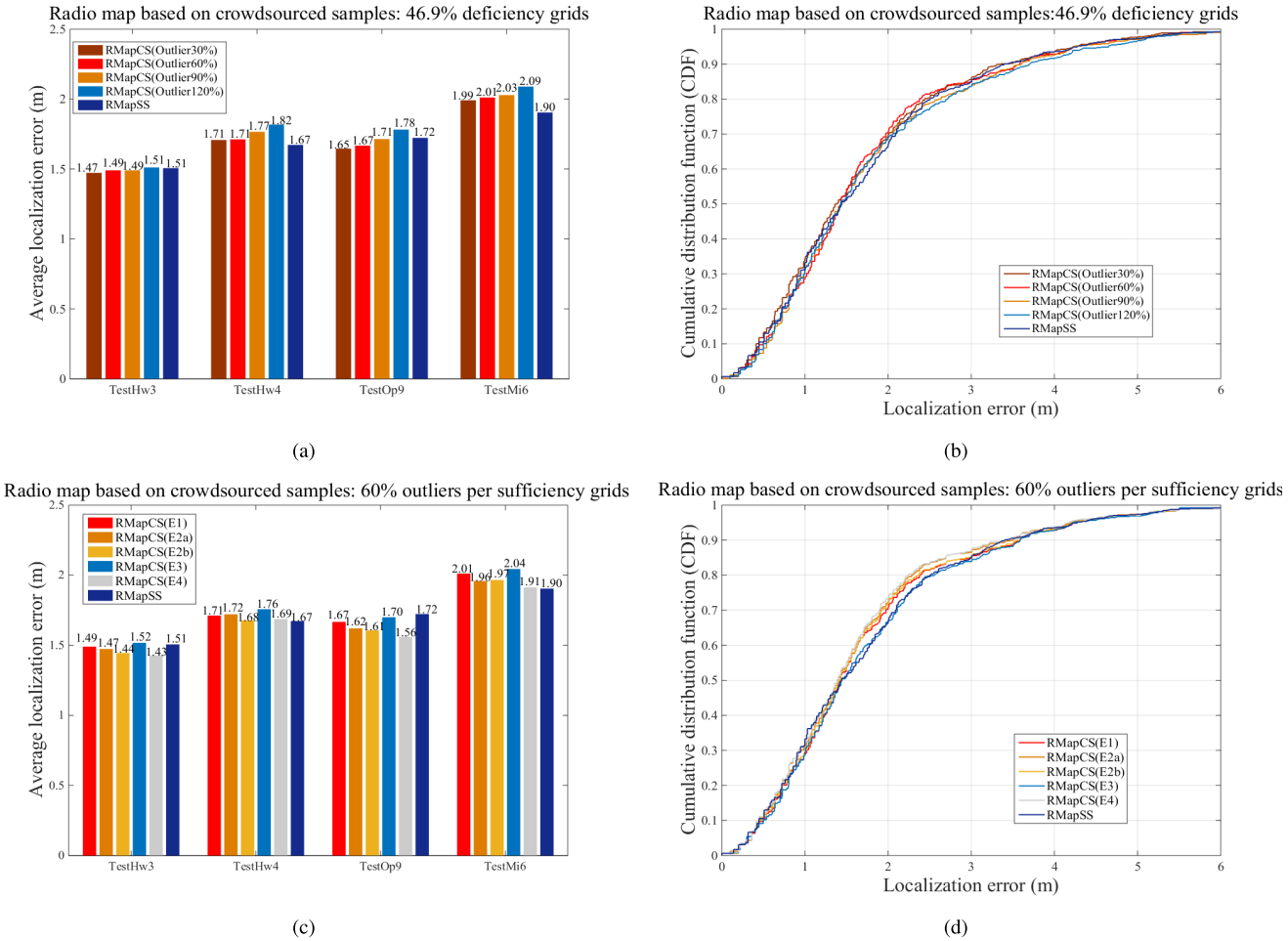

FIGURE 8. Comparison of the localization performance of RMapCS for different situations based on crowdsourced samples. (a) Localization error vs. outlier ratio for different devices. (b) Localization error CDF vs. outlier ratio. (c) Localization error vs. vacancy ratio for different devices. (d) Localization error CDF vs. vacancy ratio

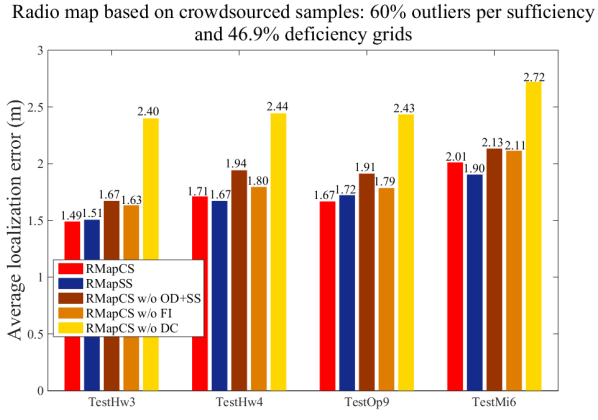

FIGURE 9. Comparison of ALE based on crowdsourced samples.

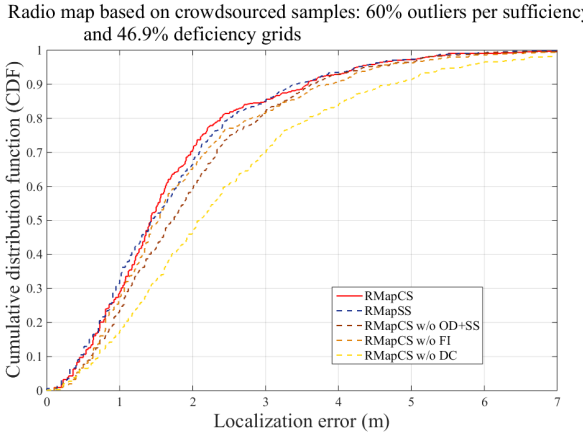

FIGURE 10. Comparison of CDF based on crowdsourced samples.

outliers are selected from the training samples in those grids whose centers are from 1m to 5m away from the given grid center. Different radio maps can be constructed based on the choices of grid sample support set. Furthermore, the testing fingerprints can be constructed either for each device or for all devices. In the former case, we construct four device-specific testing datasets. In the latter case, we construct a single device-mixed testing dataset that still contains 650 testing fingerprints, yet each one-quarter being randomly selected from per-device fingerprints.

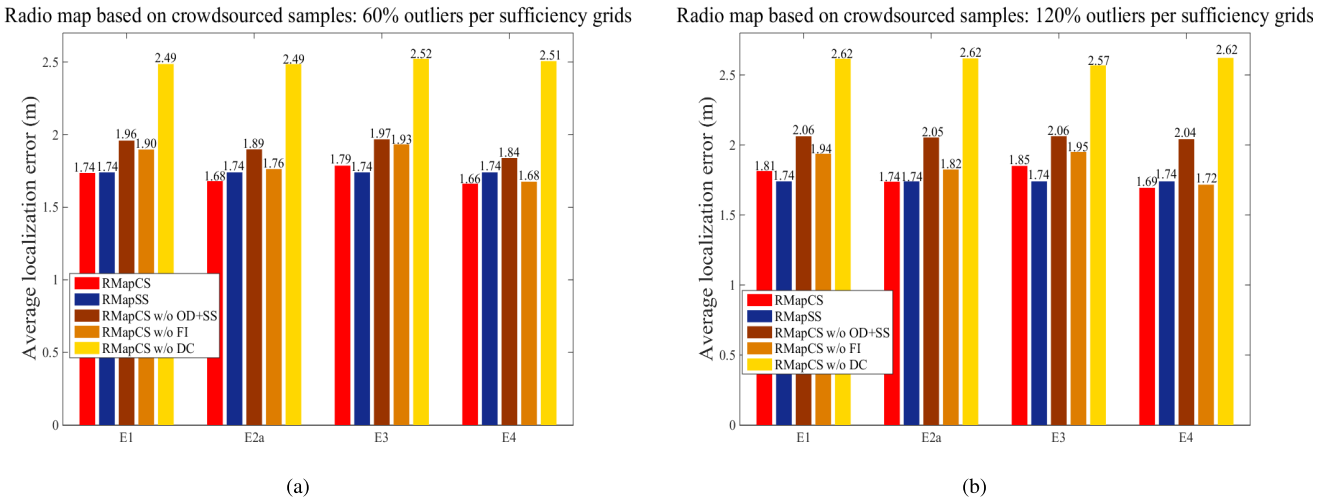

FIGURE 11. Comparison of ALE for the device-mixed testing dataset based on crowdsourced samples with four situations including (E1), (E2a), (E3) and (E4) when some of its modules are disabled. (a) Localization error vs. vacancy ratio for different schemes (60% outlier case). (b) Localization error vs. vacancy ratio for different schemes (120% outlier case)

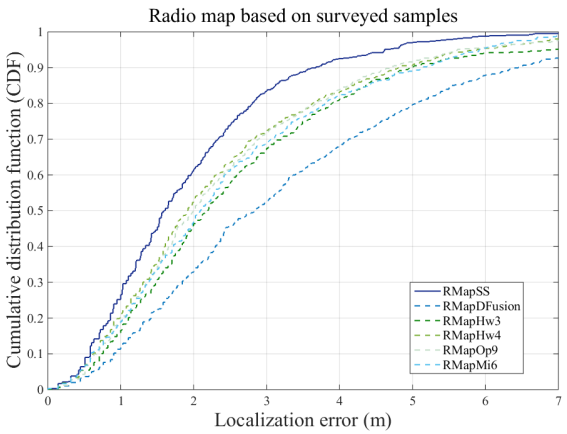

FIGURE 12. Comparison of CDF of Mx5 based on surveyed samples.

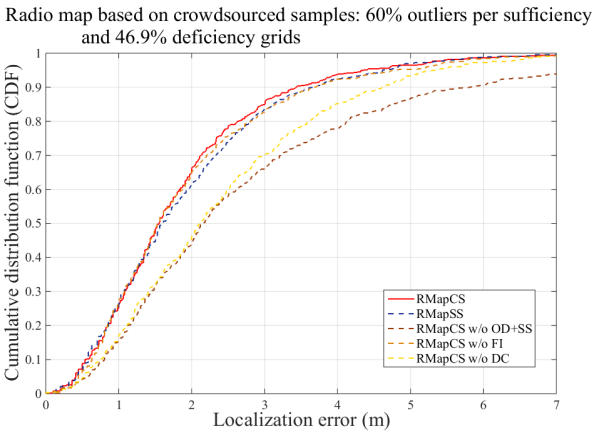

FIGURE 13. Comparison of CDF of Mx5 based on crowdsourced samples.

B. EXPERIMENT RESULTS

1) PERFORMANCE COMPARISON BASED ON SURVEYED SAMPLES

We note that our proposed scheme can also be applied to the site survey approach to construct a radio map, denoted as RMapSS. Since each grid contains only surveyed samples yet from different devices, we mainly examine its capability to deal with the device diversity challenge. For comparison, we also construct radio maps for each device based on its own surveyed samples, called RMapHw3, RMapHw4, RMapOp9 and RMapMi6. Furthermore, we construct a radio map based on a simple device fusion algorithm that obtain the averaged RSS values over the surveyed samples from all the four devices, denoted by RMapDFusion.

Fig. 5 plots the *average localization error* (ALE) of these radio maps for the four device-specific testing datasets, and Fig. 6 plots the *cumulative distribution function* (CDF) of localization errors for the device-mixed testing dataset. It can be observed that our RMapSS achieves the best localization performance in both types of testing datasets. In particular, its improvements over those of RMapDFusion are 30.1%, 19.3%, 39.6% and 48.7%, respectively, in the four device-specific testing dataset. In the construction of RMapSS, since each training sample is obtained within a specific grid and all grids contain enough training samples, we only execute the device calibration module to deal with the issue of training samples from different devices. The results validate the effectiveness of our device calibration algorithm.

2) RMapCS PERFORMANCE BASED ON CROWDSOURCED SAMPLES

We first compare the performance of the iterative with one-time outlier detection. Fig. 7 plots the main classification results where the deficiency ratio is set as 46.9%. We first observe that, no matter the iterative or onetime outlier detection in all devices, the more outliers, the worse of the

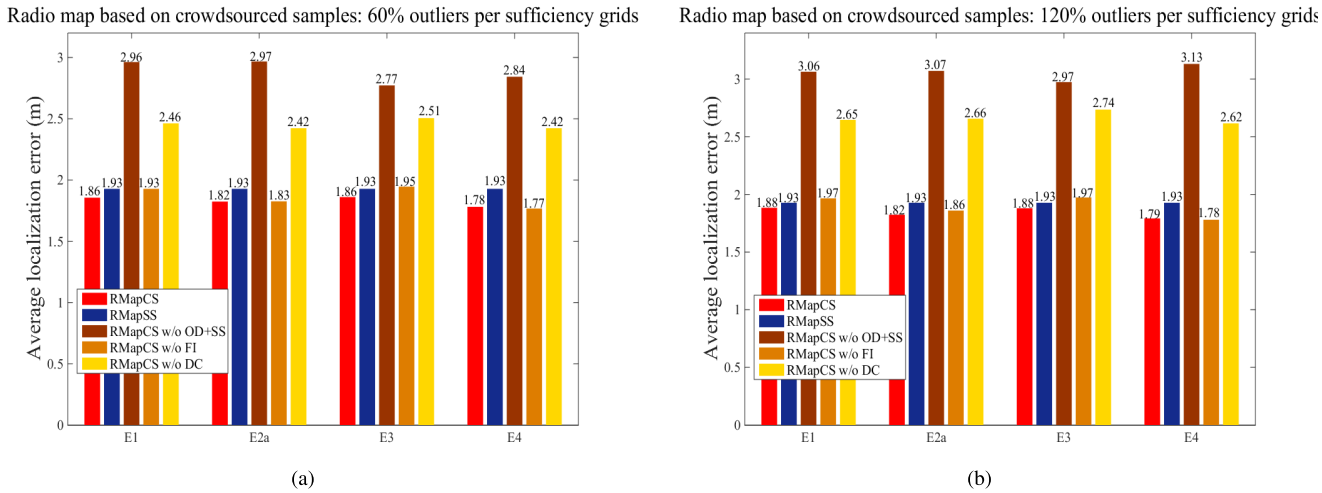

FIGURE 14. Comparison of ALE of Mx5 based on crowdsourced samples with four situations including (E1), (E2a), (E3) and (E4) when some of its modules are disabled. (a) Mx5 localization error vs. vacancy ratio for different schemes (60% outlier case). (b) Mx5 localization error vs. vacancy ratio for different schemes (120% outlier case)

classification performance of Accuracy and Precision. This is because, within a given range, as the number of outliers increases, the local density of outliers will increase, which results in more outliers being divided into normal samples. Furthermore, it can be seen that the iterative one can achieve a higher precision yet with a lower recall. In our problem, we would rather remove a normal being detected as an outlier, than including an outlier being detected as normal. The results suggest that, comparing with the onetime outlier detection, the iterative one removes some normal samples, but more outliers are removed, which meets our design objective.

We next examine the localization performance of RMapCS for different situations of obtaining crowdsourced samples. We mainly consider two practical cases: The ratio of outliers in sufficiency grids and the ratio of deficiency grids. To this end, we include different numbers of outliers into each sufficiency grid. Furthermore, we create deficiency grids according to the practical situations. As illustrated in Fig. 4, we consider the following five situations. (E1) (46.9%): The middle of corridor and sides of four rooms; (E2a) (34.4%) The corridor and sides of room 213 and 216 and full rooms 214 and 215; (E2b) (34.4%) The corridor and sides of room 214 and 215 and full rooms 213 and 216; (E3) (25%) The corridor and sides of four rooms; (E4) (21.9%) The middle of corridor and full four rooms. The number in the bracket indicates the radio of deficiency grids.

Fig. 8 (a) and (b) plot the localization performance when the outlier ratio increases in each sufficiency grid, where the deficiency ratio is set as 46.9%. Fig. 8 (c) and (d) plot the localization performance for different ratios of deficiency grids, where the outlier ratio is set as 60%. It is not unexpected to observe that the localization performance degrades with the increase of outlier ratio and deficiency grids. When the outlier ratio increases, it becomes harder to detect and remove all outliers from the support set. The localization hence would suffer from those unremoved outliers, as they also take part in the radio map construction. When observing Fig. 8 (c) and (d), the performance of (E4) is slightly better than the other situations, as it contains the fewest deficiency grids requiring fingerprint interpolation. On the other hand, we can observe that the performance degradation is not significant from the CDF results in the four device-specific testing dataset in these practical scenarios. The results could validate the robustness of our proposed scheme.

Then we examine the RMapCS performance when some of its modules are disabled for a typical situation of 60% outlier ratio and 46.9% deficiency grids. Fig 9 plots the average localization error for the four device-specific testing datasets, and Fig. 10 plots the CDF of localization errors for the device-mixed testing dataset. Furthermore, we compare the performance for the device-mixed testing dataset based on crowdsourced samples for four situations including (E1), (E2a), (E3) and (E4) when some of its modules are disabled. Fig 11(a) and Fig 11(b) plot the average localization error with 60% and 120% outliers per sufficiency grid, respectively. It can be observed that the localization performance suffers with the removal of one or more modules from the proposed RMapCS. On the other hand, it is interesting to see that the proposed scheme with the crowdsourced samples achieves a similar localization performance compared with the surveyed samples, i.e., RMapCS vs. RMapSS, in both testing datasets. The results validate the effectiveness of not only each proposed module but also the whole scheme for radio map construction.

3) PERFORMANCE COMPARISON FOR THE NEW DEVICE DATASET

In many practical cases, it could happen that an online testing fingerprint is from a new device that has not been used in the offline radio map construction. We next use the testing fingerprints from the another smartphone Mx5 to examine the applicabilitiness of a radio map. Fig. 12 and Fig. 13,

respectively, compares the localization error CDF for different radio maps by using the surveyed samples for the proposed scheme by using crowdsourced samples. It can be observed that the proposed scheme RMapSS outperforms all the others in terms of lower localization errors. In particular, the ALE improvements of **RMapSS** are 29.3%, 19.9%, 22.2%, 22.5% over the device-specific radio map of **RMapHw3**, **RMapHw4**, **RMapOp6**, **RMapMi6**, respectively, and 43.1% over the device fusion scheme **RMapDFusion**. Furthermore, we compare the performance of Mx5 based on crowdsourced samples for four situations including **(E1)**, **(E2a)**, **(E3)** and **(E4)** when some of its modules are disabled. Fig 11(a) and Fig 11(b) plot the average localization error with 60% and 120% outliers per sufficiency grid, respectively. The results validate the applicableness of the proposed scheme.

VI. CONCLUSION

In this paper, we have proposed a **RMapCS** scheme which contains four offline modules and one improved online positioning algorithm to deal with the four challenges when constructing a radio map from crowdsourced samples. Field measurements and experiments have validated the effectiveness, robustness and applicableness of the proposed scheme. In our future work, we shall further study the update strategy for grid support set and indoor radio map when receiving newly crowdsourced samples.

REFERENCES

[1] B.-F. Wu and C.-L. Jen, "Particle-filter-based radio localization for mobile robots in the environments with low-density WLAN APs," *IEEE Trans. Ind. Electron.*, vol. 61, no. 12, pp. 6860–6870, Dec. 2014.

[2] P. Lin, Q. Li, Q. Fan, X. Gao, and S. Hu, "A real-time location-based services system using WiFi fingerprinting algorithm for safety risk assessment of workers in tunnels," *Math. Problems Eng.*, vol. 2014, Feb. 2014, Art. no. 371456.

[3] R. Harle, "A survey of indoor inertial positioning systems for pedestrians," *IEEE Commun. Surveys Tuts.*, vol. 15, no. 3, pp. 1281–1293, 3rd Quart., 2013.

[4] M. Zhang, Y. Wen, J. Chen, X. Yang, R. Gao, and H. Zhao, "Pedestrian dead-reckoning indoor localization based on OS-ELM," *IEEE Access*, vol. 6, pp. 6116–6129, 2018.

[5] S. He and S.-H. G. Chan, "Wi-Fi fingerprint-based indoor positioning: Recent advances and comparisons," *IEEE Commun. Surveys Tuts.*, vol. 18, no. 1, pp. 466–490, 1st Quart., 2015.

[6] B. Wang, Q. Chen, L. T. Yang, and H.-C. Chao, "Indoor smartphone localization via fingerprint crowdsourcing: Challenges and approaches," *IEEE Wireless Commun.*, vol. 23, no. 3, pp. 82–89, Jun. 2016.

[7] Z. T. Mu Zhou, Y. Wei, X. Yang, and L. Li, "Achieving cost-efficient indoor fingerprint localization on wlan platform: A hypothetical test approach," *IEEE Access*, vol. 6, pp. 15865–15874, 2017.

[8] K. Chang and D. Han, "Crowdsourcing-based radio map update automation for Wi-Fi positioning systems," in *Proc. ACM SIGSPATIAL Int. Workshop Crowdsourced Volunteered Geograph. Inf.*, 2014, pp. 24–31.

[9] B. Wang, S. Zhou, W. Liu, and Y. Mo, "Indoor localization based on curve fitting and location search using received signal strength," *IEEE Trans. Ind. Electron.*, vol. 62, no. 1, pp. 572–582, Jan. 2015.

[10] B. Wang, S. Zhou, L. Yang, and Y. Mo, "Indoor positioning via subarea fingerprinting and surface fitting with received signal strength," *Pervasive Mobile Comput.*, vol. 23, no. 2, pp. 23–48, 2015.

[11] M. Zhou, Q. Zhang, Y. Wang, and Z. Tian, "Hotspot ranking based indoor mapping and mobility analysis using crowdsourced Wi-Fi signal," *IEEE Access*, vol. 5, pp. 3594–3602, 2017.

[12] S.-H. Jung, S. Lee, and D. Han, "A crowdsourcing-based global indoor positioning and navigation system," *Pervasive Mobile Comput.*, vol. 31, pp. 94–106, Sep. 2016.

[13] S.-H. Jung, B.-C. Moon, and D. Han, "Unsupervised learning for crowdsourced indoor localization in wireless networks," *IEEE Trans. Mobile Comput.*, vol. 15, no. 11, pp. 2892–2906, Nov. 2016.

[14] C. Wu, Z. Yang, and Y. Liu, "Smartphones based crowdsourcing for indoor localization," *IEEE Trans. Mobile Comput.*, vol. 14, no. 2, pp. 444–457, Feb. 2015.

[15] Y. Kim, H. Shin, Y. Chon, and H. Cha, "Crowdsensing-based Wi-Fi radio map management using a lightweight site survey," *Comput. Commun.*, vol. 60, pp. 86–96, Apr. 2015.

[16] M. Zhou, Y. Tang, Z. Tian, and X. Geng, "Semi-supervised learning for indoor hybrid fingerprint database calibration with low effort," *IEEE Access*, vol. 5, pp. 4388–4400, 2017.

[17] Z. Huang, J. Xia, H. Yu, Y. Guan, X. Gan, and J. Liu, "Fusing fixed and hint landmarks on crowd paths for automatically constructing Wi-Fi fingerprint database," *China Commun.*, vol. 12, no. 1, pp. 11–24, 2015.

[18] H. Abdelnasser *et al.*, "SemanticSLAM: Using environment landmarks for unsupervised indoor localization," *IEEE Trans. Mobile Comput.*, vol. 15, no. 7, pp. 1770–1782, Jul. 2016.

[19] L. Li, G. Shen, C. Zhao, T. Moscibroda, J.-H. Lin, and F. Zhao, "Experiencing and handling the diversity in data density and environmental locality in an indoor positioning service," in *Proc. ACM MobiCom*, 2014, pp. 459–470.

[20] Y. Ye and B. Wang, "Indoor radio map construction based on crowdsourced fingerprint splitting and fitting," in *Proc. IEEE Wireless Commun. Netw. Conf. (WCNC)*, Mar. 2017, pp. 1–6.

[21] E. Laitinen and E.-S. Lohan, "Are all the access points necessary in WLAN-based indoor positioning?" in *Proc. IEEE Localization GNSS (ICL-GNSS)*, Jun. 2015, pp. 1–6.

[22] D. Liang, Z. Zhang, and M. Peng, "Access point reselection and adaptive cluster splitting-based indoor localization in wireless local area networks," *IEEE Internet Things J.*, vol. 2, no. 6, pp. 573–585, Dec. 2015.

[23] H.-N. Manh, C.-C. Huang, and H.-Y. Lee, "Auto-calibration for device-diversity problem in an indoor localization system," in *Proc. IEEE Int. Conf. Consum. Electron.-Taiwan (ICCE-TW)*, Jun. 2015, pp. 78–79.

[24] H.-C. Yen and C.-C. Wang, "Cross-device Wi-Fi map fusion with Gaussian processes," *IEEE Trans. Mobile Comput.*, vol. 16, no. 1, pp. 44–57, Jan. 2017.

[25] J.-G. Park, D. Curtis, S. Teller, and J. Ledlie, "Implications of device diversity for organic localization," in *Proc. IEEE INFOCOM*, Apr. 2011, pp. 3182–3190.

[26] J. Ledlie *et al.*, "Mole: A scalable, user-generated WiFi positioning engine," in *Proc. IEEE Int. Conf. Indoor Positioning Indoor Navigat.*, Sep. 2011, pp. 1–10.

[27] C. Laoudias, D. Zeinalipour-Yazti, and C. G. Panayiotou, "Crowdsourced indoor localization for diverse devices through radiomap fusion," in *Proc. IEEE Indoor Positioning Indoor Navigat. (IPIN)*, Oct. 2013, pp. 1–7.

[28] F. Dong, Y. Chen, J. Liu, Q. Ning, and S. Piao, "A calibration-free localization solution for handling signal strength variance," in *Mobile Entity Localization and Tracking in GPS-Less Environnments* (Lecture Notes in Computer Science), vol. 5801, R. Fuller and X. D. Koutsoukos, Eds. Berlin, Germany: Springer, 2009, pp. 79–90, doi: doi.org/10.1007/978-3-642-04385-7_6.

[29] M. B. Kjærgaard and C. V. Munk, "Hyperbolic location fingerprinting: A calibration-free solution for handling differences in signal strength (concise contribution)," in *Proc. IEEE Int. Conf. Pervasive Comput. Commun. (PerCom)*, Mar. 2008, pp. 110–116.

[30] M. B. Kjærgaard, "Indoor location fingerprinting with heterogeneous clients," *Pervasive Mobile Comput.*, vol. 7, no. 1, pp. 31–43, 2011.

[31] A. K. M. M. Hossain, Y. Jin, W.-S. Soh, and H. N. Van, "SSD: A robust RF location fingerprint addressing mobile devices' heterogeneity," *IEEE Trans. Mobile Comput.*, vol. 12, no. 1, pp. 65–77, Jan. 2013.

[32] H. Zou, B. Huang, X. Lu, H. Jiang, and L. Xie, "A robust indoor positioning system based on the procrustes analysis and weighted extreme learning machine," *IEEE Trans. Wireless Commun.*, vol. 15, no. 2, pp. 1252–1266, Feb. 2016.

[33] S. Yang, P. Dessai, M. Verma, and M. Gerla, "FreeLoc: Calibration-free crowdsourced indoor localization," in *Proc. IEEE INFOCOM*, Apr. 2013, pp. 2481–2489.

[34] Y. Jiang *et al.*, "Ariel: Automatic Wi-Fi based room fingerprinting for indoor localization," in *Proc. ACM Conf. Ubiquitous Comput.*, 2012, pp. 441–450.

[35] Y. Shu *et al.*, "Gradient-based fingerprinting for indoor localization and tracking," *IEEE Trans. Ind. Electron.*, vol. 63, no. 4, pp. 2424–2433, Apr. 2016.

[36] A. Rodriguez and A. Laio, "Clustering by fast search and find of density peaks," *Science*, vol. 344, no. 6191, pp. 1492–1496, Jun. 2014.

YANZHEN YE received the B.S. degree from the School of Electronic Information and Communications, Huazhong University of Science and Technology, Wuhan, China, in 2016, where she is currently pursuing the master's degree. Her research interests include indoor localization technology and systems.

BANG WANG received the B.S. and M.S. degrees from the Department of Electronics and Information Engineering, Huazhong University of Science and Technology (HUST), Wuhan, China, in 1996 and 2000, respectively, and the Ph.D. degree from the Department of Electrical and Computer Engineering, National University of Singapore, in 2004. He is currently a Professor with the School of Electronic Information and Communications, HUST. He has authored or co-authored over 100 technical papers in international conferences and journals. His research interests include wireless networking issues, indoor localization systems, and social computing technologies.